According to previous discussions, parametric shimmy will occur as the value of a in Eqs. (16) approaches unity, i.e., when the velocity of the vehicle reaches the following two critical values:

$$V_{cr,1} \approx 80.6 \text{ mph}, \; V_{cr,2} \approx 448.5 \text{ mph} \qquad (18)$$

The two principal unstable regions of Eq. (14) are shown in Fig. 2. q in Fig. 2 is defined in Eq. (16).

To demonstrate the phenomenon of the parametric shimmy and to evaluate the approximations in Eq. (11), we have numerically integrated the original Eq. (6), by using the values in Eq. (17). The results are given in Figs. 3a and 3b. Figure 3a shows the camber α and shimmy θ motions of the gear when the vehicle travels at its first critical speed $\approx$80.6 mph. Note, at this speed, the frequency of the wheel unbalance force is approximately 18 cps, while the unstable motions of both camber and yaw are oscillating at 9 cps—the fundamental natural frequency of the system. Observed also in Fig. 3a, the shimmy motion θ, at the beginning, has a tendency to oscillate at its own natural frequency (50 cps); but gradually moves with the camber motion as α grows. Similar phenomena are found at the second critical speed ($\approx$448 mph), where α moves with the yaw θ, and the gear is also unstable (Fig. 3b).

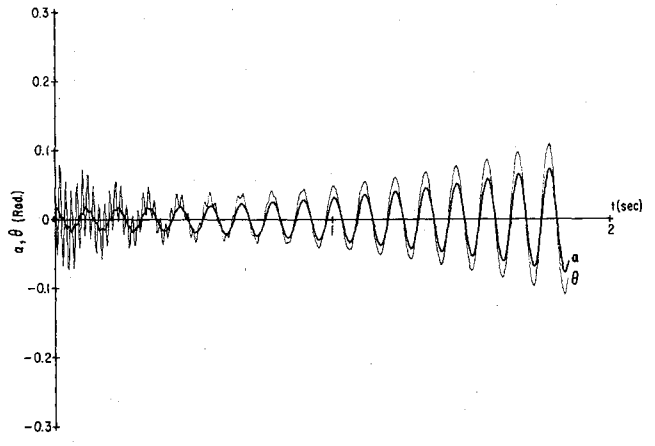

Fig. 3a Shimmy and camber motions of the nosegear (at V = 80.6 mph).

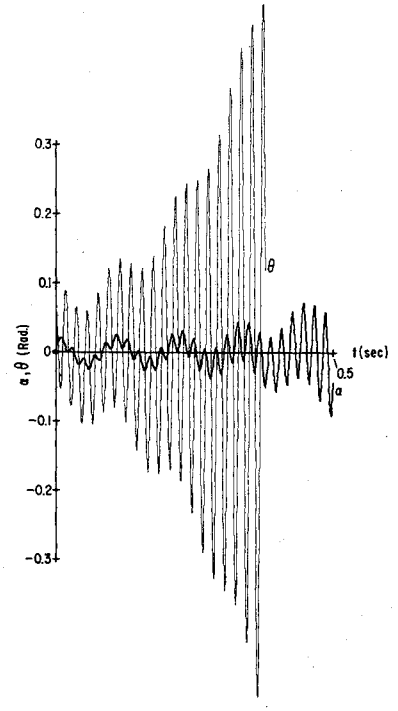

Fig. 3b Shimmy and camber motions of the nosegear (at V = 448.5 mph).

The parametric shimmy shown in Fig. 3a and 3b is obviously of a self-excited type. In a real gear system where damping is used, this shimmy is possible only when the wheel imperfection is so significantly large that the actual q value in Eq. (16) will fall into the instability region of a damped Mathieu equation,[4,5] in the vicinity of the critical speeds. Also in the present gear model, the parametric shimmy will not occur when the trail length L is zero.

References

[1] Von Schlippe, B. and Dietrich, R., "Shimmying of a Pneumatic Wheel," TM-1365, Aug. 1954, NACA, pp. 125–160.

[2] Moreland, W. J., "The Story of Shimmy," *Journal of the Aeronautical Sciences*, Vol. 21, No. 12, Dec. 1954, pp. 793–808.

[3] Smiley, R. F., "Correlation, Evaluation, and Extension of Linearized Theories for Tire Motion and Wheel Shimmy," TN-3632, June 1956, NACA.

[4] Hayashi, C., *Nonlinear Oscillations in Physical Systems*, McGraw-Hill, New York, 1964.

[5] Bolotin, V. V., *The Dynamic Stability of Elastic Systems*, Holden-Day, San Francisco, Calif., 1964.

Lower Bounds for Sonic Boom Considering the Negative Overpressure Region

James S. Petty*
Aerospace Research Laboratories, Wright-Patterson Air Force Base, Ohio

THE possible inapplicability of the asymptotic sonic boom theory for large SST-type aircraft, particularly during the critical transonic acceleration flight condition, was noted by McLean.[1] Subsequently, the nonasymptotic theory has been utilized to obtain configurations with considerably lower boom overpressures than earlier believed possible. Reasoning similar to that used by Jones[2,3] may be used to obtain lower bound configurations from the nonasymptotic theory if only the positive overpressure is of interest.[4] However, unlike the asymptotic overpressure signature the nonasymptotic signature is not, in general, antisymmetric about its midpoint and, in particular, the magnitude of the negative peak overpressure may be larger than the positive peak overpressure. Therefore, it is necessary to consider both the positive and negative parts of the overpressure signature when seeking lower bound configurations from the nonasymptotic theory. In the analysis that follows, we draw heavily on the definitive paper of Whitham[5] and on those of Jones and Walkden.[6]

We assume that the aircraft may be replaced by the equivalent area distribution $A_e(x) = S(x) + \beta L(x)/\rho V^2$, for $x < l$, where $S(x)$ is the cross-sectional area distribution, $L(x)$ is the integral of the longitudinal lift distribution, and l is the over-all aircraft length. For $x > l$ the distribution $A_e(x) = A_e(l) \equiv A_{e,b}$ is assumed. If the equivalent distribution is smooth and slender, then A_e and Whitham's function F are related by the Abel transform pair

$$A_e(x) = 4 \int_0^x F(y)(x - y)^{1/2} dx \qquad (1)$$

Received January 7, 1970; revision received May 30, 1970.
* Aerospace Engineer, Hypersonic Research Laboratory. Member AIAA.

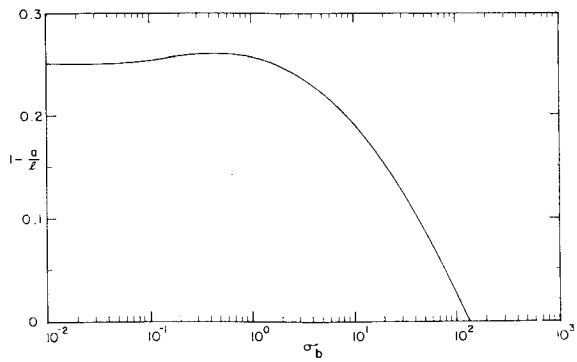

Fig. 1 $1 - \alpha/l$ vs nondimensional base area.

$$F(y) = \frac{1}{2\pi}\int_0^x A_e''(x)(y-x)^{-1/2}dx \tag{2}$$

assuming $F(0) = A_e(0) = A_e'(0) = 0$. In a uniform atmosphere, the pressure signature at a vertical distance h below the aircraft is given by $\Delta p/p = [\gamma/(\gamma+1)](\beta/M^2)[kF(y)/h^{1/2}]$ and $x - \beta h = y - kh^{1/2}F(y)$, where $k = 2^{-1/2}(\gamma+1)M^4\beta^{3/2}$. If regions exist in which $x(y)$ is multivalued, shocks must be placed to make $x(y)$ single valued. Across a shock we have, with $y_1 < y_2$

$$kh^{1/2}[F(y_2) - F(y_1)] = y_2 - y_1 \tag{3}$$

$$\frac{1}{2}(y_2 - y_1)[F(y_2) + F(y_1)] = \int_{y_1}^{y_2} F(y)dy \tag{4}$$

with the subsidiary condition $F'(y_1) \geqq F'(y_2)$. For the front shock, $F(y_1) = 0$, so the previous reduces to

$$\frac{1}{2}kh^{1/2}F^2(y_0) = \int_0^{y_0} F(y)dy \tag{5}$$

with $y_0 > 0$.

In order to consider the negative overpressure region, the strength of the aft shock must be found, which requires knowledge of the distribution $F(y)$ for $y > l$. Since $A_e''(x) = 0$ for $x > l$,

$$F(y) = \frac{1}{2\pi}\int_0^l A_e''(x)(y-x)^{-1/2}dx$$

for $y > l$. The area distribution may be eliminated using Eq. (1) to give

$$F(y) = -\frac{1}{\pi}\int_0^l F(\eta)\left[\frac{l-\eta}{y-l}\right]^{1/2}\frac{d\eta}{y-\eta} \tag{6}$$

for $y > l$. Since there may be a "corner" at $x = 1$, i.e., $A_e'(x)$ discontinuous, Eqs. (1) and (2), and thus also Eq. (6), will not, in general, be valid in the neighborhood of $x = l$. This possible invalidity will be ignored for the moment and discussed later. The equations for the aft shock may be obtained now if the corner at $x = l$ is assumed convex and if it is assumed that $y_1 = l$ in Eqs. (3) and (4). After some manipulation, the aft shock relations are found to be

$$F(y_1) = \frac{y_2 - l}{kh^{1/2}} - \frac{1}{\pi}\int_0^l F(y)\left[\frac{l-y}{y_2-l}\right]\frac{dy}{y_2-y} \tag{7}$$

$$0 = \frac{(y_2-l)}{kh^{1/2}} + \frac{2}{\pi}\int_0^l F(y)\times \left[\frac{(l-y)^{1/2}(y_2-l)^{1/2}}{y_2-y} - 2\tan^{-1}\left(\frac{y_2-l}{l-y}\right)^{1/2}\right]dy \tag{8}$$

For a given $F(y)$, the previous equations may be solved for y_2 and $F(y_1)$. Since these equations are sufficiently complex that the effect on $F(y_1)$ of a change in $F(y)$ is not obvious, it is useful to introduce a small variation δF and ascertain its effect. This may be shown to be

$$\delta F(y_1) = -\frac{2}{\pi y_2}\int_0^l \tan^{-1}\left(\frac{y_2-l}{l-y}\right)^{1/2}\delta F(y)dy \tag{9}$$

Finally, we note from Eq. (1) that the equivalent base area is

$$A_{e,b} = 4\int_0^l F(y)(l-y)^{1/2}dy \tag{10}$$

A lower bound distribution may now be obtained as follows: 1) It follows from Eqs. (9) and (10) that, in order to maximize $A_{e,b}$ and minimize $|F(y_1)|$, the positive area under $F(y)$ should be concentrated as near $y = 0$, and the negative area as near $y = l$, as possible. 2) The front shock terminates at y_0 as defined by Eq. (5) and the overpressure immediately behind it is given by $F(y_0)$. Between the shocks the distribution must be such that $F(y_0) \geqq F(y) \geqq F(y_1)$. 3) If $F(y_0)$ is fixed, then by Eq. (5) the area

$$\int_0^{y_0} F(y)dy$$

is also fixed, independent of y_0. Therefore, statement 1 indicates that y_0 should be chosen as small as possible ($y_0 \to \epsilon \ll l$). 4) From the previous, the optimum should be

$$F(y) = \frac{1}{2}\frac{kh^{1/2}}{l}F^2(y_0)\delta\frac{y-\epsilon}{l} + F(y_0) - [F(y_0) - F(y_1)]H(y-\alpha) \tag{11}$$

for $0 \leqq y < l$, where $\delta(z)$ is a Dirac delta function, $H(z)$ is the Heaviside unit function, and α is a constant to be determined by the requirement that the magnitude of the peak negative overpressure must not be greater than the peak positive overpressure, i.e., $|F(y_1)| \leqq F(y_0)$. If this distribution is substituted into Eqs. (7, 8, and 10), a set of three nonlinear algebraic equations is obtained that may be solved numerically to obtain $A_{e,b}, y_2$, and either $F(y_1)$ or α as functions of $F(y_0)$.

The results of the numerical computations are shown in the figures, where the following nondimensional variables are used: $\sigma_b = k(h/l)^{1/2}A_{e,b}/l^2$ and $\Delta\pi = \beta^{-1/4}(h/l)^{3/4}(A_{e,b}/l^2)^{-1/2}|\Delta p/p|$.

In Fig. 1, the variation of α and σ_b is presented for the condition $F(y_1) = -F(y_0)$. As can be seen, $(1 - a/l)$ decreases to zero for σ_b of about 131. For $\sigma_b > 131$, $(1 - \alpha/l)$ is zero and, for $F(y)$ given by Eq. (11), the trailing shock is weaker than the leading shock.

The nondimensional peak overpressure magnitude $\Delta\pi$ for the present lower bound solution is presented in Fig. 2. For comparison, we have also included the asymptotic lower bound solution of Jones and the solution for the lower bound of the peak positive overpressure [given by setting $\alpha = l$ in Eq. (11)]. Seebass[4] and A. R. George have also derived

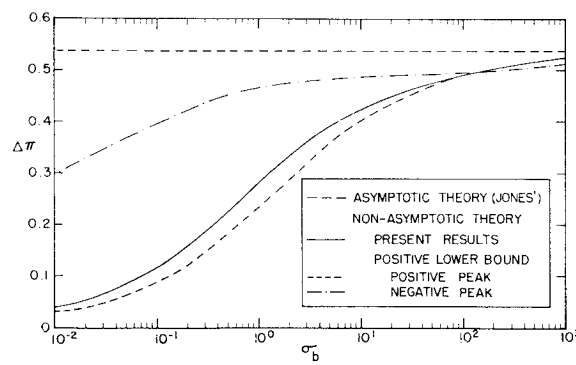

Fig. 2 Peak overpressure magnitudes from several lower bound analyses.

this latter result. For this case, the peak negative overpressure magnitude is also presented to illustrate the importance of the negative overpressure region. As can be seen, consideration of both positive and negative overpressures results in a large decrease in peak negative overpressure magnitude with a relatively small penalty in peak positive overpressure.

Several assumptions were made following Eq. (6) that need some comment. The possible invalidity of $F(y)$ just behind the "corner" at $x = l$ is of no great concern since this region is cut off by the rear shock and only the integral of $F(y)$, which is given accurately by our approximate form, is needed. Our results show that the "corner" at $x = l$ is indeed convex for all σ_b, becoming smooth for $\sigma_b \to 0$, which confirms a posteriori our assumption. The assumption that, for the lower bound configuration, we should choose $y_1 = l$ at the rear shock is more difficult to justify in a simple manner. Suffice it to note that variational analysis indicates that $y_1 = l$ gives at least a relative bound.

The results presented above assume a uniform atmosphere. The effects of a stratified atmosphere on sonic boom have been treated by George and Plotkin[7] in a manner which can be easily applied to the previous results by a simple redefinition of the nondimensional variables σ_b and $\Delta\pi$. Using George's coefficients C_I, C_A, and C_T, if we redefine

$$\sigma_b = k\left(\frac{h}{l}\right)^{1/2}\frac{A_{e,b}}{l^2}\left(\frac{\gamma}{\gamma+1}\frac{\beta}{M}C_T\frac{c}{h^{1/2}}\right)$$

$$\Delta\pi = \beta^{-1/4}\left(\frac{h}{l}\right)^{3/4}\left(\frac{A_{e,b}}{l^2}\right)^{-1/2}\left|\frac{\Delta p}{p}\right| C_I C_A \times \left(\frac{h}{l}\right)^{1/2}\left(\frac{\gamma}{\gamma+1}\frac{\beta}{M}C_T\frac{c}{h^{1/2}}\right)^{1/2}$$

where c is the sonic speed at the altitude of the aircraft, the results presented in Figs. 1 and 2 are also valid for stratified atmospheres.

As an example, we show in Fig. 3 the lower bound equivalent area and F distributions for an SST aircraft 300 ft long and weighing 50,000 lb, flying at Mach 1.414 at 40,000 ft in a standard atmosphere. This corresponds to $\sigma_b = 0.3$ and has a peak overpressure magnitude of 0.74 psf on the ground (assuming a reflection coefficient of 2).

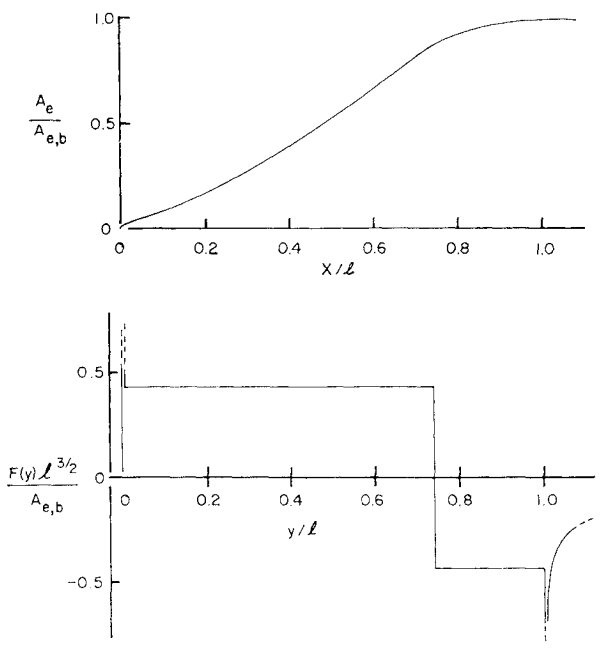

Fig. 3 Lower bound configuration for $l = 300$ ft, $w = 5 \times 10^5$ lb, $M = 1.414$, $h = 4 \times 10^4$ ft.

For comparison between the present results and those of Seebass, we consider a 600,000-lb aircraft which is 300 ft long and flying at 60,000 ft at Mach 2.7 in an atmosphere with a scale height of 20,000 ft. Our results show a peak overpressure magnitude of 1.19 psf compared with Seebass' result of 1.04 psf for the positive overpressure only (which corresponds to the lower curve in Fig. 2) and about 1.5 psf for his antisymmetrical signature. The present results indicate that, although it may be necessary to consider the negative overpressure region in configuration tailoring for sonic boom, the penalty incurred in doing so should not be large.

References

[1] McLean, F. E., "Some Nonasymptotic Effects on the Sonic Boom of Large Airplanes," TN D-2877, June 1965, NASA.

[2] Jones, L. B., "Lower Bounds for Sonic Bangs," *Journal of the Royal Aeronautical Society*, Vol. 65, No. 606, June 1961, pp. 433–436.

[3] Jones, L. B., "Lower Bounds for Sonic Bangs in the Far Field," *The Aeronautical Quarterly*, Vol. 18, Feb. 1967, pp. 1–21.

[4] Seebass, R., "Sonic Boom Theory," *Journal of Aircraft*, Vol. 6, No. 3, May–June 1969, pp. 177–184.

[5] Whitham, G. B., "The Flow Pattern of a Supersonic Projectile," *Communications in Pure and Applied Mathematics*, Vol. 5, Aug. 1952, pp. 301–348.

[6] Walkden, F., "The Shock Pattern of a Wing-Body Combination, Far from the Flight Path," *The Aeronautical Quarterly*, Vol. 9, Pt. II, May 1958, pp. 164–194.

[7] George, A. R. and Plotkin, K. J., "Sonic Boom Waveforms and Amplitudes in a Real Atmosphere," *AIAA Journal*, Vol. 7, No. 10, Oct. 1969, pp. 1978–1981.

Generation of Erroneous Line-of-Sight Rates by Radome Refraction Errors

Carl Grubin*
Hughes Aircraft Company, Culver City, Calif.

Introduction

A SIGNIFICANT measurement error for a radar system located in a tracking aircraft can be developed as a result of refraction of the beam as it passes through the radome. The time derivative of this refraction error creates, in effect, an erroneous line-of-sight rate of the target as seen by the radar. The purpose of this Note is to derive this error.

Analysis

The airborne radar carried in aircraft A tracks some target T, usually another aircraft or possibly a ground target. Designate the unit vector along the actual geometric line-of-sight (LOS) from A to T by $\bar{\imath}$. If $\dot{\bar{\imath}} \equiv (d\bar{\imath}/dt)$ is the derivative as seen in a nonrotating coordinate system centered at the interceptor, the true line-of-sight rate (LOSR) is

$$\bar{\Omega} = \bar{\imath} \times \dot{\bar{\imath}} \tag{1}$$

If the radome refraction error is δ, the apparent LOS lies along $\bar{\imath}'$ where $\bar{\imath}'$ is deflected from $\bar{\imath}$ by angle δ (Fig. 1).

From Fig. 1

$$\bar{\imath}' = \bar{\imath} + \Delta\bar{\imath} \tag{2}$$

where, since δ is small (e.g., less than 1°)

$$|\Delta\bar{\imath}| = \delta, \text{ in rads} \tag{3}$$

Received March 10, 1970.

* Senior Staff Engineer, Aeronautical Systems Division. Associate Fellow AIAA.